Magnetic tomography for lead acid batteries

Harry T. Harrison*, Glynn Cooke, David A. Hewitt, David A. Stone, James E. Green, Member IEEE

The Department of Electronic and Electrical Engineering, University of Sheffield, 3 Solly Street, Sheffield S1 4DE, UK

A B S T R A C T

This paper explores the inverse problem approach for finding the current distribution within an electrochemical cell from magnetic field measurements. Current distribution is shown to be a useful measurement for diagnosis of cells and development of cell design. Existing current distribution measurement methods are discussed to provide context and motivation for the work. Magnetic field measurements can be obtained non-invasively and contain information about the current distribution, which is extracted using an appropriate solver. Experimental results are presented which test the effectiveness of a particular inverse problem solver, using both simulated and real magnetic field measurements. The solver presented is based upon one found in literature, but with novel problem-specific modifications. Errors in conductance values in the forward model definition are simulated in order to quantify their effect on solution quality. A modification to the solver is proposed to improve robustness against these model errors. This results in improved solution quality when using real measured data from a resistor-wire model of a cell, and simulated data from a model which more accurately represents the conductance of the cell plate grid and active mass.

1. Introduction

The hybridisation and electrification of vehicles requires high performance batteries in terms of energy density and specific energy [1], high current delivery (cold and warm cranking) [2], long service life [3], and dynamic charge acceptance [4]. In addition, cost of the batteries must be minimised [1] to bring the price of electric vehicles and hybrid electric vehicles to a level that is competitive with internal combustion engine vehicles. It should be noted that the wide variety of levels of hybridisation (plug-in hybrid, mild hybrid, micro-mild hybrid *etc.*) yields an equally wide variety of battery requirement specifications [4,5]. Even in purely internal combustion engine-powered vehicles, stop-start functions as well as more sophisticated power management place more demand on the battery than in the traditional starting-lighting-ignition application [4]. Uniformity of current distribution has been shown to be a factor contributing to various measures of battery performance, which are described in Section 2.

For the purposes of this paper, current distribution refers to the current leaving or entering the plate due to the cell reaction. Furthermore, distribution over the whole area of the cell plate (mesoscopic) is of interest, as opposed to what happens at the microscopic level, or how current may be shared between multiple cells within a battery or batteries within a battery pack (macroscopic). In other words the goal is to produce a diagram showing the regions of greater and lesser magnitude of current over the whole area of the cell plate (see Figs. 3, 5, 7, 8). This does not imply that the micro- or macro- scopic models of the battery system are not related, but the mechanisms at those levels are beyond the scope of this paper.

We investigate the use of magnetic measurement for imaging the current distribution within lead acid cells. Using magnetic measurements to obtain current distribution is applicable to many battery chemistries, but automotive lead acid cells are a convenient choice for experimentation due to their relatively large plate size and the fact that they are available dry-charged, allowing safe construction of a test cell. Despite being a mature technology, research into lead acid batteries is ongoing. This is because they are commercially relevant due to their low cost [6,7], but have limited dynamic charge acceptance [4] and poor specific energy. Firstly, the motivation for the research is explained in Section 2, and a very brief description is provided of the ways in which current distribution impacts on some battery performance metrics. Then, a review of the existing methods for measuring the current distribution in lead acid cells is provided (Section 3). This includes some related methods, with comment on their applicability. The

* Corresponding author.
  E-mail address: elp13hth@shef.ac.uk (H.T. Harrison).

review also includes some background for magnetic imaging as a method. Finally, some experimental work is presented (Section 4) which is concerned with finding the current distribution from magnetic field measurements using an inverse problem approach.

2. Current distribution, cell performance and state of health

2.1. Dynamic charge acceptance

Inhomogeneous current density distribution has been linked with reduced dynamic charge acceptance [8]. It is offered as an explanation for the dependence of dynamic charge acceptance on the recent charging/discharging history of the battery, which has also been reported in [9]. Acid stratification is suggested as the cause of the inhomogeneous current distribution, since it is dependent on recent history of the battery. Acid stratification also causes premature sulphation in localised areas of the battery plate, even at modest overall depth of discharge for the whole cell [10]. This is acknowledged as a failure mechanism in lead acid cells [8,11,12] Sunu and Burrows use potential non-uniformity around the plate as a figure of merit for cell performance [13].

2.2. Active mass utilisation

One factor determining the specific energy of a battery is the active mass utilisation – lead acid batteries in practice perform poorly in this regard compared to other battery chemistries (such as nickel metal-hydride (NiMH) and lithium ion (Li-Ion)), and also compared to the theoretical maximum specific energy for a lead acid battery [14–16]. Active mass utilisation is typically measured by taking the time integral of the current at the battery terminals, and measuring the mass of the active material, giving a capacity in units of Ah kg_{AM}^{-1} [17]. The theoretical capacity of a given mass of active material is obtained by considering the atomic weights of Pb and/or PbO_2 and the number of atoms needed to exchange an electron at each electrode [18]. By measuring localised current density, a localised measure of active mass utilisation is possible [19]. A non-uniform active mass utilisation means that some parts of the plate are underutilised (resulting in poor specific energy) and some parts are over-utilised (resulting in damage due to deep discharge [20]). In addition, the mechanisms themselves which limit active mass utilisation are current-dependent; it has been found that the dominant process limiting active mass utilisation depends on the rate of charge/discharge (at high rates transport of acid through the active mass limits its utilisation [21] whereas at low rates it is the electronic conductivity of the active mass [15,16]). Therefore knowledge of current distribution will give greater insight into the mechanisms governing the active mass utilisation at different locations around the cell plate. Gyenge et al. [17] develop a novel current collector for lead acid batteries with improved active mass utilisation compared to a standard grid. They acknowledge that current distribution measurements could aid optimisation of active mass thickness.

2.3. State of health

As well as optimising performance, information on current distribution of a cell could be used to identify damage or wear to the cell. Active mass shedding, where the active mass falls from the plates and pools in the bottom of the battery case, is one failure mechanism for lead acid batteries. A summary of aging and failure of lead acid batteries by Ruetschi [10] gives examples of a plate which has shed its active mass over part of its area. Areas where active mass are not present would not be able to participate in the cell reaction and so there would be no current leaving the plate in these areas. Two other failure modes from the same paper are

firstly, capacity loss due to poor contact between the active mass and supporting grid and secondly, short circuiting between plates due to movement of active mass. If the former occurs initially in one part of the plate area, then a reduced current density would be expected in that part of the cell, and so a current distribution measurement may be useful for showing the degradation of the plate by this method. In the latter case, short circuits occur towards the bottom of the cell due to shedding, or elsewhere around the plate if dendrites are formed [10]. Identifying the path of the short circuit current would differentiate between these two cases. Sulphation is another cause of capacity loss and failure, which may occur non-uniformly on battery plates, with a distribution that is dependent on charge/discharge rate [11,22,23].

3. Existing current distribution measurement methods

There is relatively little experimental (as opposed to simulation) work on the current distribution of lead acid batteries. However, similar research into fuel cells is much more active. Kalvyas et al. [24] provide a review of methods for measuring current distribution in polymer electrolyte fuel cells. Some techniques used in fuel cells are applicable to lead acid batteries, but not all. This is because the geometry of a fuel cell or flow battery can be more complex than a lead acid battery – it may include multiple layers, and a convoluted flow channel to transport the fuel around the electrode [25,26]. By contrast, the cell of a parallel plate lead acid battery, such as those used for starting, lighting and ignition of an internal combustion engine vehicle, consists of two opposing faces of adjacent plates of approximately similar geometry with an absorbed aqueous or gelled electrolyte in between. The cell is then simply repeated and connected in series/parallel to increase the battery voltage/current. One plate may form part of either one or two cells, since the active mass may be pasted onto both faces of the plate, but the geometry of each cell is simple and repeating.

3.1. Modelling

Lead acid batteries have been modelled as electrochemical and as purely resistive systems. Newman and Tiedemann [27] develop a macrohomogeneous theory of the cell reactions, which is used by Kowal et al. in their study into current inhomogeneity and recent cycle history of a lead acid cell [8]. Sunu and Burrows incorporate a resistive model of the plate grids into an electrochemical model of the battery in order to predict potential and current density distributions [13,19] and the effect of altering grid design. Due to the relative ease/speed of creating models compared to building a real grid, the authors were able to make comparisons between various proposed grid designs and dimensions in order to plot capacity against grid weight – aiding optimisation of specific energy. Král et al. [28] developed an equivalent circuit incorporating resistances of constituent parts of a lead acid cell as well as the state of charge-dependent local polarisations to simulate non-uniformity of current distribution for different battery current take-off tab configurations.

3.2. Sense wires

One direct way to measure potential distribution around the plate (and thereby estimate current distribution by making assumptions about the resistivity of the electrolyte) is to attach sense wires to the grid. Calabek et al. constructed a purely resistive model from a pair of unpasted lead acid cell plate grids, connected together by uniformly spaced resistance wires to simulate the electrolyte resistance. Using this apparatus they found that the uniformity of the current distribution can be improved by correct

placement of the current take-off tabs [29]. Schulte et al. [11] connected four sense wires to the vertical edge of the negative plate grid, leaving most of the active mass in place. This allows indirect measurement of current distribution (assuming current distribution is uniform horizontally) in conjunction with pH measurements to identify acid stratification. Current distribution became less uniform after 1000 micro-cycles. The transient behaviour of the voltage dropped between the different measurement points allows comparison of the varying charge acceptance at different heights on the plate as well as the current distribution.

Both the sense wire-based methods described are highly invasive – they both require alteration to the battery plates. Schulte's method only provides 4 voltages which can be subtracted from each other, so only 3 regions between which current can be compared. Attaching more wires over the plate area would in principle be possible but re-pasting the plate, or some method of preserving the active mass, would be necessary in order to observe normal operation of the cell. Calabek's experimental setup is less comprehensive than similar simulated models. For example, it doesn't include the time-varying potentials that occur during a charge/discharge. However, it does provide some useful experimental verification for other investigations into tab placement such as [28,29] and is qualitatively in agreement with both the results of both those studies.

3.3. Reference electrodes

A tool widely used to analyse electrolytic systems is the reference electrode. This is an electrode which has a known potential in the electrolyte of interest. They are often used to measure the potential of an unknown electrode. Newman and Tiedemann [30] describe taking reference electrode measurements at various points around a cell to obtain potential and current distribution. Reference electrodes have also been used by Guo et al.[31,32] in a pair to measure the resistive voltage drop across the electrolyte when a current is passed through a lead acid cell. The voltage drop is proportional to the electrolytic current which passes from close to the first reference electrode to close to the second. The authors assumed that electrolyte conductance was uniform and constant. By scanning the pair of electrodes in tandem around the cross sectional area of the cell, the local current across the cross sectional area can be found [31,32].

The use of reference electrodes is less invasive than the sense wire method, as the cell plates themselves do not have to be modified. However, the plate separation must be much greater than that found in a commercial automotive lead acid battery in order to fit either one or two standard reference electrodes in between the plates, plus clearance for scanning the electrode position if a scanning method is being employed. An electrode which would fit into a 1–2 mm gap between plates has been created especially for research into lead acid batteries [33], but has not been used in a scanning application. Like all scanning methods, there is a trade-off between spatial resolution of the current distribution image and the time taken to acquire the image. A further disadvantage of scanning electrodes in the region between the plates is that is makes it difficult to compress the active mass in order to improve plate lifetime [10]. However, reference electrode arrays have been reported for use with fuel cells [34].

3.4. Split electrodes

Another invasive method is to divide the electrodes in the cell of interest into segments in order to allow connection of an ammeter to each segment directly. The currents can then all be connected to a bus wire to complete the circuit to the battery terminal. Zhang et al. divided the positive electrode of a Li-Ion cell into 10 segments

along one dimension only, so that current from battery tab could be plotted as a function of distance [35]. The current distribution is seen to move from being mostly concentrated near to the tab at the start of a discharge (due to voltage drops accumulating as distance from the tab increases), to being mostly concentrated in the region furthest from the tab at the end of the charge (due to these regions not having been discharged as deeply as those closer to the tab). Current inhomogeneity *perpendicular* to the cell plate has been observed in a Li-Ion cell using a stack of working electrodes, giving some insight into the contribution to the reaction that is obtained by altering the thickness of the plate [36] (all the other examples in this paper are concerned with inhomogeneity in the plane *parallel* to the plates). Electrodes that are split 'in the plane' rather than stacked are commonly used in more diverse electrochemistry problems, two early examples being shown in [37,38].

A drawback to using this method in the study of batteries is that one of the electrodes must be altered significantly. Therefore only the behaviour of one electrode can be studied at a time, as is the case in [35]. The contribution to the current distribution of the electrode which has been segmented is not measured by this method. This is not a problem in some electrochemistry problems such as [37,38], where the pair of electrodes may be designed especially for the experimental setup. However, in the typical use of an automotive battery, the Ohmic potential losses in both plates can be significant contributors to current distribution [13,19,28,29] and so care must be taken when interpreting data taken from one plate only.

3.5. Magnetic resonance imaging

Some work has been undertaken on applying some established imaging techniques to batteries. Britton [39] provides a review of magnetic resonance imaging on electrically conductive and magnetically susceptible materials. This application of magnetic resonance imaging is not trivial as care must be taken to avoid eddy currents in conducting materials due to the strong magnetic fields necessary, and also distortions to the magnetic fields due to any magnetically susceptible materials present. Britton et al. [40] perform magnetic resonance imaging on a zinc-air battery cell (comprising a zinc electrode, a titanium electrode and NaOH electrolyte). By this method it is possible to identify concentrations of different chemical species in the cell, so the transport of Zn$(OH)_x^{2-}$ and OH^- ions through the electrolyte can be observed.

3.6. X-ray based methods

Pearse et al.[41] perform a 1-dimensional X-ray photoelectron spectroscopy (XPS) scan of a specially-made V_2O_5 electrode of very low width in a Li-Ion cell. Over the course of a discharge, V^{5+} ions are reduced to V^{4+}. Since these two ions exhibit different spectra, the relative concentration of the two species can be seen. The part of the electrode furthest from the tab is found to contain more V^{5+} and less V^{4+} than the part closest to the tab at the end of a discharge. Liu et al. [42] take a 45 mm x 40 mm $LiFePO_4$ electrode which has been charged to 50% SoC, and then perform an X-Ray diffraction (XRD) scan over the electrode area. The scan is able to identify the concentration of $FePO_4$ present, which is taken as a measure of local SoC. By this method, a 2-dimensional heat map plot of SoC over the electrode area is constructed, which shows a strong inhomogeneity over the electrode area. Both the X-ray based methods measure SoC distribution rather than current distribution. However these two quantities are related, since local charge is the integral of the local current. Measuring SoC can be convenient for scanning methods, as the current can be interrupted for the measurement so SoC is not changing during the scan time. The X-ray based methods are both quite low in

validity – the 2D XRD scan was conducted as a destructive test while the XPS method was only conducted along one dimension.

3.7. Flow-through magnetic sensor array

Since any electrical current will give rise to a magnetic field surrounding the current, measuring magnetic field would seem to be a convenient way of making non-contact current measurements. Indeed, standard 'clamp' current meters use a magnetic sensor as a transducer. A close relative of a clamp current meter is the current sensor array developed for measuring current distribution in a fuel cell [43]. An array of bespoke current sensors is placed between the current collector and the flow field of a large (approx. 190 mm x 300 mm) polymer electrolyte fuel cell. They are oriented to measure current transiting in or out of the current collector, with the plane of the sensor array and resulting image parallel to the current collector. Each current sensor consists of a Hall Effect magnetic field sensor, placed into an airgap cut into an annular ferrite core. Both of these components are commonly available from electronics suppliers. The ferrite provides a low reluctance path for the magnetic flux which exists due to current which passes through its centre, so that the field measured by the Hall effect sensor is a function of the local current and the size of the airgap only. A similar sensor array could in principle by applied to a parallel plate lead acid cell, although the size of the sensors reported in [43] would be too great to fit in the gap between plates in a commercial cell, and would also greatly limit resolution over the area of a typical commercial automotive battery (measured by the author as approx. 150 mm x 100 mm). An advantage of this method is that it can be used with any cell chemistry.

3.8. Magnetic tomography

The magnetic field due to the battery current also exists outside of the battery case, making a non-invasive measurement possible. Magnetic tomography is the technique of constructing an image of current distribution using external magnetic field measurements. If a current distribution is known, then the resulting magnetic field distribution may be calculated analytically (using the Biot-Savart law, Ampere's law, or Maxwell's magnetostatic equations) or by finite element methods. When calculating current distribution from the magnetic field using an inverse problem approach, the coupling between the current distribution to the magnetic field is known as the forward model. Information about both the magnetic field and the forward model is necessary to solve the inverse problem. Uniqueness must be considered when dealing with inverse problems – i.e., if a given magnetic field could have been generated by more than one current distribution, then it may be impossible to know with certainty the current distribution from magnetic field measurements. It has been shown that uniqueness exists under some conditions which are met in the case of a typical battery or fuel cell problem [44]. One constraint which makes reconstruction easier is knowledge of the position of the possible current relative to the sensors, so a model which constrains the positions and directions of the current is commonly used. 2D problems (such as the current moving around a printed circuit board) have been solved where the distance from the sensor to the plane of the currents is known [45,46]. In the study of fuel cells, quasi-2D models have been used to reconstruct current distribution by assuming negligible thickness [47,48]. If thickness is non-negligible, then a 3D model must be used. Since the position of current is no longer restricted to a planar surface, some other constraints must be imposed. One approach is to construct an electric circuit model with similar geometry and conductance distribution to the cell of interest. The magnetic field

measurements are then a function of the currents flowing in each element of the circuit model.

Hauer et al. [49] investigate methods of constraining the problem. The first method, the zero-divergence constraint, is to force the circuit to obey Kirchhoff's current law, so that the current injected at the terminals of the circuit is known and cannot disappear or be created at any of the nodes except the terminals. The second, termed 'special basis projection', is to treat the overall current distribution as a combination of the electrolyte currents, with the currents in the plates entirely determined by the electrolyte current distribution and the resistances in each branch of the circuit [49]. Both these restrictions are found to increase solution accuracy compared with a model consisting of independent elements in the same positions. However, they also both require the branch resistances to represent accurately the conductance distribution in the cell. Since some studies [13,19,28,29] have shown that the conductance distribution of the cell has a significant effect on current distribution, then this would appear to be circular reasoning. However, it has also been widely shown that current distribution changes over the course of a cycle ([8,11,19,28,32,35,41]), with the hypothesis that this is due to some areas (those close to the tabs) being preferentially charged/discharged and becoming spent prematurely, i.e. related to the charge state of the local active mass as well as the conductance distribution. One possible difficulty which remains is the conductivity of the active mass itself, which depends on SoC [15]. This means that a forward model which is accurate at 100% SoC may not be accurate at 50% SoC.

Another potential problem with constructing an accurate forward model arises when ferrous materials are consumed in the cell reaction. Any ferrous materials present in the cell under test must be also represented in the forward model as they will distort the magnetic field. In theory, if the quantity of ferrous material in the active mass is sufficient to cause significant distortion to the magnetic field, and a significant change in that quantity occurs over the course of the charge/discharge cycle then the forward model may not match the cell under test sufficiently accurately to allow solution of the problem. Apart from this potential complication, the inverse problem of solving current distribution from the magnetic field is applicable to any battery chemistry.

3.9. Sensor types and their utility in this problem

A quick estimate of the field resulting from a typical lead acid cell is given by the Biot-Savart law for a long straight wire $B_m = \frac{\mu_0 I}{2\pi r}$. B_m is magnitude of magnetic field measured by the sensor, μ_0 is the permeability of free space, I is the current and r is the perpendicular distance from the sensor to the wire.

An estimate of I is given by dividing the cold cranking amps by the number of plate pairs connected in parallel in the battery. A typical value for cold cranking amps is approximately >300 A, and a typical number of plate pairs is 10 (6x two-sided positive plates interspersed by 5x two sided negative plates, where all 10 sides of the negative plates, and all but the outer two positive plate sides take part in the cell reaction). Therefore I can be taken as 30 A. The distance from a sensor positioned next to a battery of width 200 mm must be at least 100 mm, so this can be taken as the value of r. This evaluates to give $B_m = 6 \times 10^{-5}$ T. According to a review of magnetic sensor types [50], there are a variety of sensor types available which would meet the sensitivity requirement, of which magnetoresistive sensors are probably the most readily available presently.

Green et al. captured an image of the magnetic field caused by a lead acid battery in operation using an array of magnetoresistive

sensors [51]. The low cost and size of magnetoresistive sensors means that they are well suited to magnetic sensing arrays (see also [52] for a similar array used for metal detection), allowing real-time measurements to be made. A related method (magnetoencephalography) is used in medical imaging to map neural currents. These currents cause fields of less than 1 pT and so a superconducting quantum interference device is typically used [53,54]. These are also the sensor of choice in some of the industrial applications, for example [44,45,48]. Hall effect sensors were used in the flow-through magnetic sensor array reported in [43]. These are inexpensive and compact [50], but not sensitive enough for reading the external magnetic field caused by a lead acid cell. The focussing effect of the ferrite cores used combined with the large current capacity of the cell under test meant that fields measured in [43] were much stronger.

4. Experimental work on special basis projection

In this section, the special basis projection solver method for inverse magnetostatic problems referred to in Section 3.8 and first reported in [49] is replicated, tested and adapted (Section 4.2). The usefulness of the method for imaging of a commercial lead acid cell is also investigated, by using the solver with real measured magnetic data (Section 4.3), and by simulating the conductance distribution of a typical lead acid cell plate (Section 4.4). The special basis projection method is described in more detail in Section 4.1.

4.1. Mathematical description

To discretise the unknown current distribution, the cell is represented by a 3D wire model (e.g. Fig. 1), where the positions of the nodes and branches match the dimensions of the cell. Currents may flow along any of the branches of the model, and the resulting contribution to the magnetic field at a given sensor location caused by a branch current is calculated using the information about the location of the branch relative to the sensor position.

Since there are m branches, there are m elements in $\boldsymbol{J}$, the vector which describes the current distribution. All elements of $\boldsymbol{J}$ contribute to the 3 dimensional $\boldsymbol{B}$ field at n sensor locations, so the magnetostatic system is specified by an m by $3n$ matrix $\boldsymbol{K}$. The
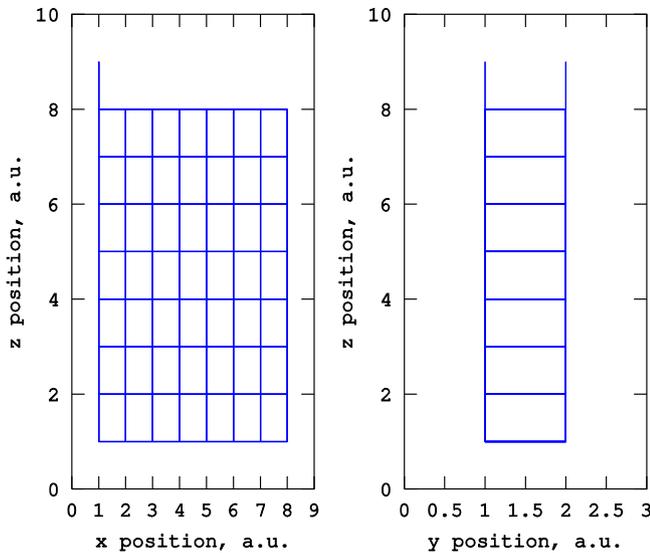
Fig. 1. A wire model giving 8×8 resolution over the plate area. Wires representing the cell plates lie in the xz plane (left). Wires representing the electrolyte lie in the y-direction, shown along with the vertical/z-direction part of the plate (right). Terminal nodes are at (1,1,9) and (1,2,9).

elements of $\boldsymbol{K}$ are numerical values calculated by evaluating the Biot-Savart law for a finite straight wire, at the appropriate dimensions and for the appropriate component of $\boldsymbol{B}$. As a matrix equation the forward model may be written as

$$\boldsymbol{B} = \boldsymbol{K}.\boldsymbol{J} \tag{1}$$

Given that measurements of $\boldsymbol{B}$ are available but $\boldsymbol{J}$ is unknown, the problem of interest is the inverse problem given by

$$\boldsymbol{J} = \boldsymbol{K}^{-1}.\boldsymbol{B} \tag{2}$$

Finding $\boldsymbol{K}^{-1}$ is considered an ill-posed problem but can sometimes be approximated using Tikhonov regularisation or a similar method. See Hofer et al. [46] for an example of using Tikhonov regularisation to approximately invert $\boldsymbol{K}$, and also how to populate the elements of $\boldsymbol{K}$ for a 2D problem. For the purposes of this paper, Tikhonov regularisation allows the approximate inversion of an ill-conditioned matrix. The degree of smoothing is determined by the regularisation parameter λ, such that a larger λ yields a smoother solution. The optimum value of λ depends on the problem, but can be determined beforehand using a range of methods [46].

Note that for the example shown in Fig. 1 there are 290 branch currents, so $\boldsymbol{K}$ must be $m = 290$ unknowns by $3n \gg 290$ measurements, so that the system is overdetermined. The complexity involved in finding $\boldsymbol{J}$ can be reduced by recognising that not all combinations of currents are valid, as the circuit must obey Kirchhoff's current law. Since it is the currents in the y direction (leaving/entering the plates) that are of interest, it is enough to consider the y direction branch currents (the elements of J_y) as independent and perform superposition of all of them to obtain the overall current distribution. Assuming that the branch resistances of the x and z wires are known, the overall current distribution in the wire model can be specified as a linear combination of the y direction currents. In matrix form this is given by [49]

$$\boldsymbol{J} = \boldsymbol{J_s}\boldsymbol{\xi} \tag{3}$$

Where $\boldsymbol{J_s}$ is a set of p partial currents where p is the number of branches pointing in the y direction, J_y. $\boldsymbol{\xi}$ is a vector (length p) specifying the weighting given to each partial solution in order to make up the actual set of branch currents, $\boldsymbol{J}$. The first column of $\boldsymbol{J_s}$ is the full list of branch currents solved for when $J_y[1] = 1$ and all other $J_y = 0$. The second row is the branch currents when $J_y[2] = 1$ and all other $J_y = 0$, and so on. Multiplying both sides of (3) by $\boldsymbol{K}$ gives

$$\boldsymbol{B} = \boldsymbol{B_s}\boldsymbol{\xi} \tag{4}$$

$$\boldsymbol{\xi} = \boldsymbol{B_s}^{-1}\boldsymbol{B} \tag{5}$$

$\boldsymbol{B}$ is obtained by measurement, and $\boldsymbol{B_s}$ by solving the forward model given by (1) for each row of $\boldsymbol{J_s}$. Finding $\boldsymbol{\xi}$ is again an ill-posed problem given by (5), albeit a less complex one than (2). $\boldsymbol{\xi}$ has size p by 1, where $p = 64$ in the example shown in Fig. 1. This method results in more stable solutions, as described by Hauer et al. [49].

4.2. Simulation of wire mesh model of cell

A solver using special basis projection is implemented in Octave, using a regularisation tools package written for Matlab [55]. λ is determined using the L-curve method [56]. Examples of reconstruction of two different current distributions are given in Fig. 2. The wire model used is the same as shown in Fig. 1. To generate the simulated measurement data R_{xyz} is set to [0.1,10,0.15]. These values are chosen such that R_y dominates, resulting in a nearly-uniform current distribution. Then, partial
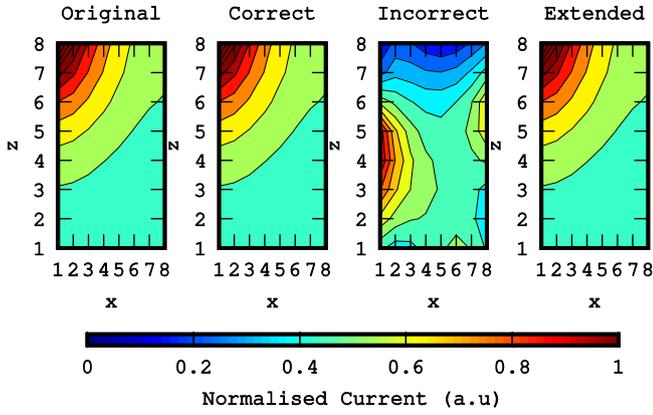
Fig. 2. An almost uniform current distribution ('Original'), and 3 reconstructions, classed by the basis used to solve. 'Correct' basis uses the same branch resistances in the solver as in the model under test. 'Incorrect' basis uses incorrect branch resistances in the solver. 'Extended' basis uses 2 sets of partial data, each with a different $\underline{r_z}$ value to allow some flexibility in the solver.

fields data are generated with the correct value of R_{xyz}. This results in good agreement with the original current distribution. This can be seen by comparison of the plots 'Original' and 'Correct' in Fig. 2. Next, partial fields data is generated where R_{xyz} is set to [0.1,10,0.1]. R_y is still much greater than R_x and R_z, so the source current distribution is not changed greatly, but the reconstruction appears highly non-uniform ('Incorrect' plot, Fig. 2).

A way to work around an unknown in the resistance distribution is to extend the basis, by generating partial fields data for a range of possible values of R_{xyz}. In this case, the 'unknown' value of R_z can be replaced by a maximum and a minimum expected value of R_z. First, 64 partial fields are generated for $R_{xyz} = [0.1,10,0.1]$, then 64 more are generated for $R_{xyz} = [0.1,10,0.2]$. The solver can then find the weighting of all 128 partial fields to generate a solution. The result of this method is shown in the 'Extended' plot on Fig. 2.

The results show that very accurate reconstructions are possible using a special basis projection solver when no errors are present. However, the forward model used to generate partial fields must be carefully designed to match the cell under test, in order to avoid errors in reconstruction. Some tolerance can be built into the solver by extending the basis. In the example given, an error is present in only one variable in the model and so only 2 sets of p partial fields are necessary to account for it. The number of partial fields scales as $2^q p$ for p unknown y currents and q unknown model parameters, so extending the basis over many variables quickly becomes computationally expensive.

4.3. Real measurements of wire mesh model of cell

To be of any practical use the solver must be robust enough to solve the inverse problem for real measurements. A $5 \times 5 \times 2$ node circuit (Fig. 3) was constructed representing 2 parallel plates connected by an electrolyte separated into 25 segments. Resistance along each x- or z-direction branch (i.e. in the plane of the plate) was nominally 0.1 Ω, resistance along the y-direction branches was 10 Ω. The magnetic imaging system used has been previously presented in [51]. It consists of a 32×8 array of 3-axis magnetoresistive sensors over an area of approximately 432 mm x 178 mm. This geometry is chosen as it can be represented by a model similar to that shown in Fig. 1, albeit with fewer y direction branches. A standard and an extended basis solver (where R_z is allowed to vary between 0.1 Ω and 0.2 Ω) are tested. For comparison, a reconstruction using simulated data is also made.

Examples of reconstructions from the real magnetic data are given in Fig. 4. Clearly the reconstructions using real measurements (MO and MO2) are less accurate reconstructions than a simulated-only problem (OO). The region of high current density in the right of the region is reproduced more visibly in the extended basis case (MO2) than in the standard basis (MO). These observations are in agreement with measurements of mean absolute error with respect to the original current distribution (Table 1) – neither MO or MO2 are as accurate as OO, but MO2 is slightly better than MO. The advantage of extending the basis is

Fig. 3. 3D resistive circuit and magnetic sensor array used to test solver with real measured data.
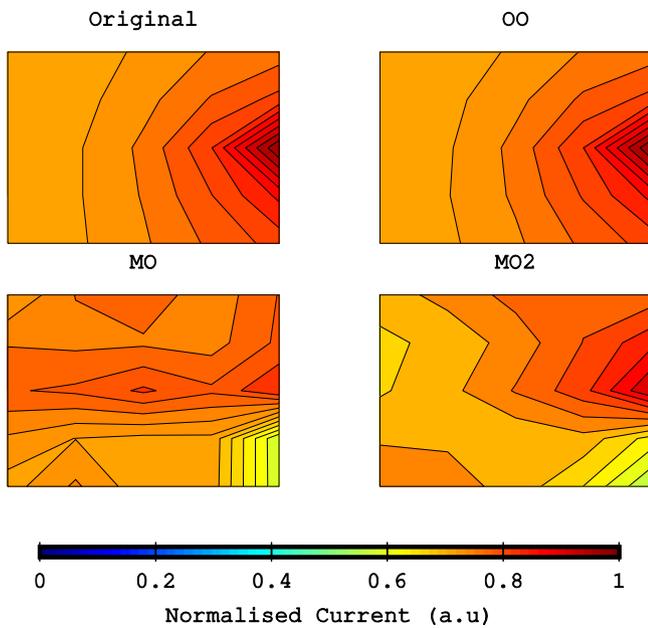
Fig. 4. A comparison between an original current distribution and its reconstructions. OO = partial fields generated in Octave to solve a simulated distribution. MO = partial fields generated in Octave to solve for real magnetic measurements. MO2 = extended basis generated in Octave to solve for real magnetic measurements.

Table 1
Mean absolute error of the 3 different problem types shown in Fig. 4.

Problem type	OO	MO	MO2
Mean absolute error, % of mean absolute value of J_y	0.14%	8.10%	5.66%

that non-ideal resistors and interconnects in the circuit can be accounted for in the solver.

4.4. Simulation of quasi-continuous model

Constructing a wire mesh which matches an electrochemical cell under test sufficiently closely, using Octave scripts, requires significant design effort. To work around this problem, it is possible to use existing finite element software to generate magnetic data from the partial current distributions. Since solution only requires inversion of the vector ξ rather than the magnetostatic coupling matrix K, then K can be replaced by some other equivalent model of which the user doesn't necessarily have explicit knowledge. We generate the set of partial magnetic fields B_s using a series of models created in an existing finite element package, which each represent one region of the electrolyte being conductive at a time. Fig. 5 shows the electrolyte segmented into 25 equal parts with the first one highlighted. The model is constructed using the graphical input of Ansys Maxwell 15.0.0. By setting one segment at a time to a nonzero conductivity and simulating the magnetic field that occurs when current is passed from one terminal to the other through the cell, a set of 25 partial magnetic fields is built up. These partial fields can then be used to solve either a simulated or a real problem with matching geometry. Model geometry is defined using a graphical input, allowing more complex geometry to be input conveniently.

To test how much of a problem unknown grid resistance might be in real measurements, a model is constructed where the plates consist of a conducting grid, with some less conductive 'active mass' surrounding the grid (Fig. 5). The grid member conductance values are taken from [13], in which a battery grid is dissected and resistances of grid members are measured. Magnetic field data is simulated from a model with the same dimensions as Fig. 5, but where the whole of the electrolyte is conducting. Partial fields are first generated from a model with accurately modelled plates, *i.e.* the same as those used to obtain the simulated data. Then partial fields are generated using a more 'naïve' model, where plates are
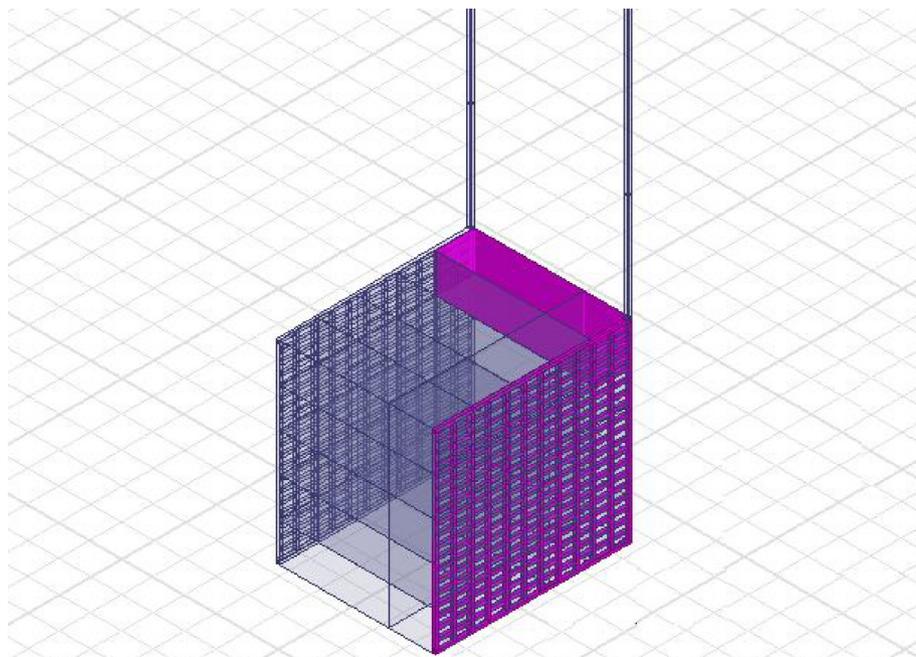
Fig. 5. Segmentation of the electrolyte and representation of the plate grid in Ansys Maxwell. One of the 25 electrolyte segments is highlighted in pink, as is one of the plate grids.
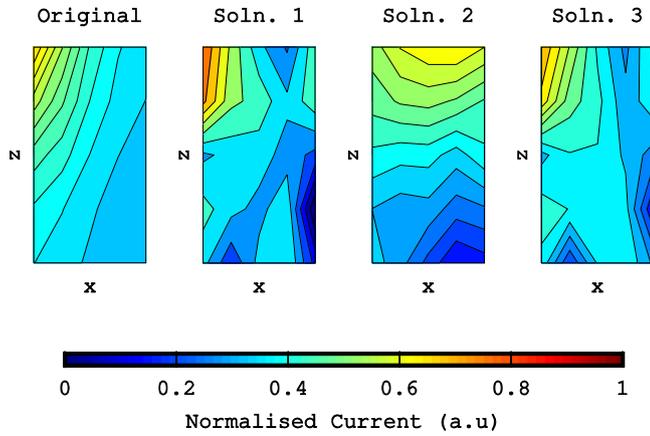
Fig. 6. Reconstructions of a uniform current distribution using Ansys as the forward model. Solution 1 uses a correct grid to generate the partial fields and a standard basis. Solution 2 uses an incorrect grid model for the partial fields. Solution 3 uses a correct grid model and a basis which is extended over a variable conductivity in the paste material. $\lambda_r = 1$.

Fig. 7. Reconstructions of a uniform current distribution using Ansys as the forward model, solution numbers same as Fig. 6. $\lambda_r = 4$.

assumed to have uniform conductivity. Finally, an extended basis model is constructed by generating partial fields for a correct grid, but for two different values of conductivity in the material surrounding the grid, which represents the lead or lead oxide active mass in a lead acid cell.

Reconstructions of a nearly-uniform current distribution are shown in Fig. 6. Again, incorrect representation of the grid in the solver causes a distorted image – notice the direction of the gradient in Solution 2 has not been reproduced accurately. Solution 3 (the extended basis) appears most similar to the original in terms of contour lines and the minimum/maximum values of current. By multiplying the value of λ calculated by the L-curve method by a constant λ_r, solutions can be over- or under- regularised. Fig. 7 shows over-regularised (*i.e.*, $\lambda_r > 1$) solutions using the same 3 solver methods. Table 2 shows the mean absolute error for the 3 solver types, and two different values of λ_r. Values of MAE in Table 2 show that over-regularisation by a factor of 4 yields better solutions in this particular problem, possibly due to the smoothness of the original current distribution. The over-regularised solutions in Fig. 7 are also more visually similar to the original than the solutions in Fig. 6.

Extending the basis over active mass conductivity could be useful in practice, since the conductivity of the grid of a lead acid cell can be measured and assumed constant, whereas the conductivity of the active mass will change as the cell reaction progresses. However since the basis is only extended over two uniform values of active mass conductivity, it is unclear how the solver will respond to non-uniform active mass conductivity.

5. Conclusion

The motivation for current distribution measurements for cell design optimisation and diagnosis is clear from the literature. In particular, treating the current distribution as the solution of an inverse problem based on a magnetostatic forward model has
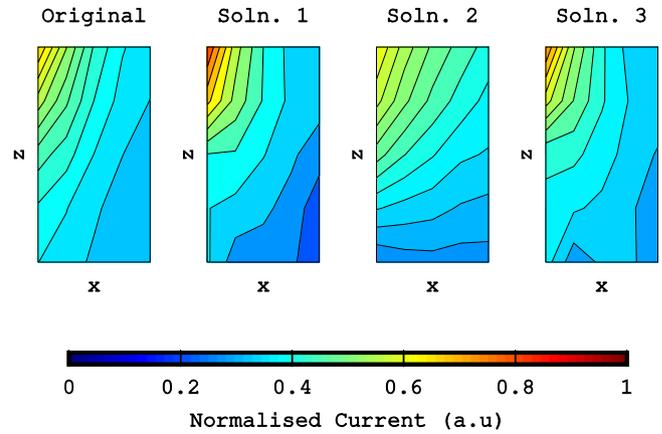
potential as a non-invasive method for measuring a range of battery chemistries. While the mathematical treatment of the inverse problem as applied to electrochemical cells can be found in the literature, there is a lack of practical examples. By focusing on applying the method to a particular cell chemistry (lead acid), we identify some of the potential challenges when applying using the inverse problem method in the real world.

We replicate the special basis projection method successfully and propose some problem-specific modifications. The tests show that the accuracy of results obtained by the solver is highly dependent on good data for the resistance distribution of the cell under test. However, some uncertainty in the model can be tolerated by extending the basis using a greater variety of partial fields. In this case two sets of fields are generated to allow variability in one of the model resistors.

An array of magnetoresistive sensors is used to measure **B** resulting from a 3D resistor-wire circuit. The solver method and the sensing system used are shown to be suitable for solution of the current distribution in the circuit from real magnetic measurements. Solution quality is improved slightly using an extended basis.

The use of a graphical finite element package as part of the solver makes accurate modelling of the cell geometry and material properties more convenient than the methods found in the literature. Some investigation is presented into the possible effect of grid and active mass conductance distribution on solution quality. In conjunction with a tear-down of a lead acid cell to obtain the resistances and dimensions of the grid members, the proposed solver could be used as part of an on-line prognostic current distribution imaging system.

Future work

Some potential difficulties in reconstructing current distribution have been identified, using simple conductive models of a lead acid cell. In order to further test the applicability of this method for real lead acid cells, it will be useful to know how these contribute

Table 2
Values of mean absolute error for the 3 solution types and 2 values of λ_r shown in Figs. 6 and 7.

Solver type	1–Correct grid in solver	2 – Grid represented as uniform material	3 – Correct grid, basis extended over active mass conductivity
Mean absolute error, % of mean absolute value of J_y; $\lambda_r = 1$	23.16%	24.23%	13.68%
Mean absolute error, % of mean absolute value of J_y; $\lambda_r = 4$	9.53%	9.01%	4.71%

and combine with other sources of error in the cell model. Further modelling with a more comprehensive model of a lead acid cell, or some real measurements on a lead acid cell will be necessary. This will give an indication as to what refinements will need to be applied to the solvers and forward models presented in this paper in order to make non-invasive measurements of current distribution with confidence. In addition, investigation of the applicability of this method to other battery chemistries would be of interest.

Funding sources

References

[1] Automotive Council UK, Driving success – a strategy for growth and sustainability in the UK automotive sector, 2013. BIS/13/975.

[2] S. Schaeck, a. O.O. Stoermer, F. Kaiser, L. Koehler, J. Albers, H. Kabza, Lead-acid batteries in micro-hybrid applications. Part I. Selected key parameters, J. Power Sources 196 (2011) 1541–1554, doi:http://dx.doi.org/10.1016/j.jpowsour.2010.08.077.

[3] H. Kiehne, Batteries for electric road vehicles, Batter. Technol. Handb, 2nd ed., Expert Verlag, 2003, 2017, pp. 149–168.

[4] E. Karden, S. Ploumen, B. Fricke, T. Miller, K. Snyder, Energy storage devices for future hybrid electric vehicles, J. Power Sources 168 (2007) 2–11, doi:http://dx.doi.org/10.1016/j.jpowsour.2006.10.090.

[5] P.T. Moseley, B. Bonnet, A. Cooper, M.J. Kellaway, Lead-acid battery chemistry adapted for hybrid electric vehicle duty, J. Power Sources 174 (2007) 49–53, doi:http://dx.doi.org/10.1016/j.jpowsour.2007.06.065.

[6] J.X. Weinert, A.F. Burke, X. Wei, Lead-acid and lithium-ion batteries for the Chinese electric bike market and implications on future technology advancement, J. Power Sources 172 (2007) 938–945, doi:http://dx.doi.org/10.1016/j.jpowsour.2007.05.044.

[7] D. Linden, T.B. Reddy, Secondary batteries – introduction, in: D. Linden (Ed.), Handb. Batter, 3rd ed., McGraw-Hill, 2002 p. 22. 1–22.24.

[8] J. Kowal, D. Schulte, D.U. Sauer, E. Karden, Simulation of the current distribution in lead-acid batteries to investigate the dynamic charge acceptance in flooded SLI batteries, J. Power Sources 191 (2009) 42–50, doi:http://dx.doi.org/10.1016/j.jpowsour.2008.12.016.

[9] D.U. Sauer, E. Karden, B. Fricke, H. Blanke, M. Thele, O. Bohlen, J. Schiffer, J.B. Gerschler, R. Kaiser, Charging performance of automotive batteries-an underestimated factor influencing lifetime and reliable battery operation, J. Power Sources 168 (2007) 22–30, doi:http://dx.doi.org/10.1016/j.jpowsour.2006.11.064.

[10] P. Ruetschi, Aging mechanisms and service life of lead-acid batteries, J. Power Sources 127 (2004) 33–44, doi:http://dx.doi.org/10.1016/j.jpowsour.2003.09.052.

[11] D. Schulte, T. Sanders, W. Waag, J. Kowal, D.U. Sauer, E. Karden, Automatic device for continuous measurement of potential distribution and acid stratification in flooded lead-acid batteries, J. Power Sources 221 (2013) 114–121, doi:http://dx.doi.org/10.1016/j.jpowsour.2012.07.072.

[12] R. Kaiser, Optimized battery-management system to improve storage lifetime in renewable energy systems, J. Power Sources 168 (2007) 58–65, doi:http://dx.doi.org/10.1016/j.jpowsour.2006.12.024.

[13] W.G. Sunu, B.W. Burrows, Mathematical model for design of battery electrodes I. Potential distribution, J. Electrochem. Soc. 129 (1982) 688, doi:http://dx.doi.org/10.1149/1.2123952.

[14] R. Ponraj, S.D. McAllister, I.F. Cheng, D.B. Edwards, Investigation on electronically conductive additives to improve positive active material utilization in lead-acid batteries, J. Power Sources 189 (2009) 1199–1203, doi:http://dx.doi.org/10.1016/j.jpowsour.2008.12.077.

[15] H. Metzendorf, The capacity limiting role of the electronic conductivity of the active material in lead-acid batteries during discharge, J. Power Sources 7 (1982) 281–291, doi:http://dx.doi.org/10.1016/0378-7753(82)80017-7.

[16] D.B. Edwards, S. Zhang, Influence of different aspect ratio additives on the performance of lead-acid batteries, J. Power Sources 135 (2004) 297–303, doi:http://dx.doi.org/10.1016/j.jpowsour.2004.03.081.

[17] E. Gyenge, J. Jung, S. Splinter, A. Snaper, High specific surface area, reticulated current collectors for lead–acid batteries, J. Appl. Electrochem. (2002) 287–295.

[18] D. Pavlov, Calculation of the active materials for lead-acid cells, Lead-Acid Batter Sci. Technol., Elsevier B.V., 2011, pp. 607–622.

[19] W. Sunu, B. Burrows, Mathematical model for design of battery electrodes II. Current density distribution, J. Electrochem. Soc. (1984).

[20] T. Huang, W. Ou, B. Feng, B. Huang, M. Liu, W. Zhao, Y. Guo, Researches on current distribution and plate conductivity of valve-regulated lead-acid batteries, J. Power Sources 210 (2012) 7–14, doi:http://dx.doi.org/10.1016/j.jpowsour.2012.02.086.

[21] P.T. Moseley, Positive plate additives, J. Power Sources 64 (1997) 47–50, doi:http://dx.doi.org/10.1016/S0378-7753(96)02499-8.

[22] M.L. Soria, F. Trinidad, J.M. Lacadena, J. Valenciano, G. Arce, Spiral wound valve-regulated lead-acid batteries for hybrid vehicles, J. Power Sources 174 (2007) 41–48, doi:http://dx.doi.org/10.1016/j.jpowsour.2007.04.035.

[23] L.T. Lam, N.P. Haigh, C.G. Phyland, A.J. Urban, Failure mode of valve-regulated lead-acid batteries under high-rate partial-state-of-charge operation, J. Power Sources 133 (2004) 126–134, doi:http://dx.doi.org/10.1016/j.jpowsour.2003.11.048.

[24] C. Kalyvas, A. Kucernak, D. Brett, G. Hinds, S. Atkins, N. Brandon, Spatially resolved diagnostic methods for polymer electrolyte fuel cells: a review, Wiley Interdiscip. Rev. Energy Environ. 3 (2014) 254–275, doi:http://dx.doi.org/10.1002/wene.86.

[25] M. Winter, R.J. Brodd, What are batteries, fuel cells, and supercapacitors? Chem. Rev. 104 (2004) 4245–4269, doi:http://dx.doi.org/10.1021/cr020730k.

[26] J.T. Clement, D.S. Aaron, M.M. Mench, In situ localized current distribution measurements in all-Vanadium redox flow batteries, J. Electrochem. Soc. 163 (2016) A5220–A5228, doi:http://dx.doi.org/10.1149/2.029305jes.

[27] J. Newman, W. Tiedemann, Porous-electrode theory with battery applications, AIChE J. 21 (1975) 25–41, doi:http://dx.doi.org/10.1002/aic.690210103.

[28] P. Král, P. Křivák, P. Bača, M. Calábek, K. Micka, Current distribution over the electrode surface in a lead-acid cell during discharge, J. Power Sources 105 (2002) 35–44, doi:http://dx.doi.org/10.1016/S0378-7753(01)00923-5.

[29] M. Calabek, K. Micka, P. Baca, P. Krivak, Influence of grid design on current distribution over the electrode surface in a lead-acid cell, J. Power Sources 85 (2000) 145–148.

[30] J. Newman, W. Tiedmann, Potential and current distribution in electrochemical cells, J. Electrochem. Soc. 140 (1993) 1961–1968.

[31] Y. Guo, W. Li, L. Zhao, A study of current and potential distributions on tubular positive plate, J. Power Sources 116 (2003) 193–202, doi:http://dx.doi.org/10.1016/S0378-7753(02)00691-2.

[32] Y. Guo, Y. Li, G. Zhang, H. Zhang, J. Garche, Studies of current and potential distributions on lead-acid batteries: I. Discharge of automotive flooded positive plates, J. Power Sources 124 (2003) 271–277, doi:http://dx.doi.org/10.1016/S0378-7753(03)00768-7.

[33] M.K. Carpente, D.M. Bemardi, J. a Wertz, The use of Hg/Hg2SO4 reference electrodes in valve-regulated lead/acid cells, J. Power Sources 63 (1996) 15–22.

[34] P.C. Rieke, Thin film electrode arrays for mapping the current-voltage distributions in proton-exchange-membrane fuel cells, J. Electrochem. Soc. 134 (1987) 1099, doi:http://dx.doi.org/10.1149/1.2100623.

[35] G.S. Zhang, C.E. Shaffer, C.-Y.Y. Wang, C.D. Rahn, In-situ measurement of current distribution in a Li-Ion cell, J. Electrochem. Soc. 160 (2013) A610–A615, doi:http://dx.doi.org/10.1149/2.046304jes.

[36] S.-H. Ng, F. La Mantia, P. Novák, P. Novak, P. Novák, P. Novak, A multiple working electrode for electrochemical cells: a tool for current density distribution studies, Angew. Chem. Int. Ed. Engl. 48 (2009) 528–532, doi:http://dx.doi.org/10.1002/anie.200803981.

[37] W.W. Focke, On the mechanism of transfer enhancement by eddy promoters, Electrochim. Acta 28 (1983) 1137–1146, doi:http://dx.doi.org/10.1016/0013-4686(83)80019-X.

[38] L.R. Czarnetzki, L.J.J. Janssen, Electrode current distribution in a hypochlorite cell, J. Appl. Electrochem. 19 (1989) 630–636, doi:http://dx.doi.org/10.1007/BF01320637.

[39] M.M. Britton, Magnetic resonance imaging of electrochemical cells containing bulk metal, ChemPhysChem 15 (2014) 1731–1736, doi:http://dx.doi.org/10.1002/cphc.201400083.

[40] M.M. Britton, P.M. Bayley, P.C. Howlett, A.J. Davenport, M. Forsyth, In situ, real-time visualization of electrochemistry using magnetic resonance imaging, J. Phys. Chem. Lett. 4 (2013) 3019–3023, doi:http://dx.doi.org/10.1021/jz401415a.

[41] A.J. Pearse, E. Gillette, S.B. Lee, G.W. Rubloff, The reaction current distribution in battery electrode materials revealed by XPS-based state-of-charge mapping, Phys. Chem. Chem. Phys. 18 (2016) 19093–19102, doi:http://dx.doi.org/10.1039/c6cp03271k.

[42] J. Liu, M. Kunz, K. Chen, N. Tamura, T.J. Richardson, Visualization of charge distribution in a lithium battery electrode, J. Phys. Chem. Lett. 1 (2010) 2120–2123, doi:http://dx.doi.org/10.1021/jz100634n.

[43] E. Gulzow, C. Wieser, a Helmbold, A new technique for two-dimensional current distribution measurements in electrochemical cells, J. Appl. Electrochem. 30 (2000) 803–807, doi:http://dx.doi.org/10.1023/A:1004047412066.

[44] R. Kress, L. Kuehn, R. Potthast, L. K$uuml$hn, R. Potthast, L. Kuhn, R. Potthast, Reconstruction of a current distribution from its magnetic field, Inverse Probl. 18 (2002) 1127–1146, doi:http://dx.doi.org/10.1088/0266-5611/18/4/312.

[45] B.J. Roth, N.G. Sepulveda, J.P. Wikswo, Using a magnetometer to image a two-dimensional current distribution, J. Appl. Phys. 65 (1989) 361–372, doi:http://dx.doi.org/10.1063/1.342549.

[46] D. Hofer, T. Wiesner, B.G. Zagar, Analyzing 2D current distributions by magnetic field measurements, 2012 IEEE Int, Instrum. Meas. Technol. Conf. Proc. 4 (2012) 2061–2066, doi:http://dx.doi.org/10.1109/I2MTC.2012.6229565.

[47] K.-H. Hauer, R. Potthast, T. Wüster, D. Stolten, Magnetotomography—a new method for analysing fuel cell performance and quality, J. Power Sources 143 (2005) 67–74, doi:http://dx.doi.org/10.1016/j.jpowsour.2004.11.054.

[48] T. Kiwa, K. Tanaka, S. Kasuya, K. Sakai, K. Tsukada, Ion transportation of electrolytes in a flow channel mapped by an HTS SQUID scanning system, IEEE Trans. Appl. Supercond. 25 (2015) 3–6, doi:http://dx.doi.org/10.1109/TASC.2014.2382656.

[49] K. Hauer, R. Potthast, M. Wannert, Algorithms for magnetic tomography—on the role of a priori knowledge and constraints, Inverse Probl. 11 (2008) 1–18, doi:http://dx.doi.org/10.1088/0266-5611/24/4/045008.

[50] J. Lenz, A.S. Edelstein, Magnetic sensors and their applications, IEEE Sens. J. 6 (2006) 631–649, doi:http://dx.doi.org/10.1109/JSEN.2006.874493.

[51] J.E. Green, D.A. Stone, M.P. Foster, A. Tennant, Spatially resolved measurements of magnetic fields applied to current distribution problems in batteries, Instrum. Meas. IEEE Trans. 64 (2015) 951–958, doi:http://dx.doi.org/10.1109/TIM.2014.2362432.

[52] D. Benitez, P. Gaydecki, S. Quek, V. Torres, Development of a solid-state multi-sensor array camera for real time imaging of magnetic fields, J. Phys. Conf. Ser. 76 (2007) 12030, doi:http://dx.doi.org/10.1088/1742-6596/76/1/012030.

[53] G. Nolte, G. Curio, On the calculation of magnetic fields based on multipole modeling of focal biological current sources, Biophys. J. 73 (1997) 1253–1262, doi:http://dx.doi.org/10.1016/S0006-3495(97)78158-X.

[54] B. Fishbine, Magnetometry harnessing the power of tiny magnetic fields, Los Alamos Res. Q. (2017) 4–11 (n.d.).

[55] P.C. Hansen, Regularization tools: a matlab package for analysis and solution of discrete ill-posed problems, Numer. Algorithms 6 (1994) 1–35.

[56] P.C. Hansen, D.P. O'Leary, The use of the L-curve in the regularization of discrete ill-posed problems, SIAM J. Sci. Comput. 14 (1993) 1487–1503, doi:http://dx.doi.org/10.1137/0914086.